



An electrochemical sensor for purine base detection with ZIF-8-derived hollow N-doped carbon dodecahedron and AuNPs as electrocatalysts

Haohong Lai¹ · Yuanyuan Niu¹ · Pingtao Ming¹ · Jinhao Wang¹ · Shumei Wang^{1,2} · Yan Xu³ · Haiyun Zhai¹

Received: 18 October 2022 / Revised: 1 December 2022 / Accepted: 7 December 2022 / Published online: 27 December 2022
© Springer-Verlag GmbH Germany, part of Springer Nature 2022

Abstract

In this paper, a novel electrochemical sensor was constructed for the detection of purine bases. Ultrafine carbide nanocrystals confined within porous nitrogen-doped carbon dodecahedrons (PNCd) were synthesized by adding molybdate to ZIF-8 followed by annealing. With MoC-based PNCds (MC-PNCds) as the carrier, gold nanoparticles (AuNPs) were deposited on the electrode surface via potentiostatic deposition as the promoter of electron transfer, forming a AuNPs/MC-PNCds/activated glassy carbon electrode (AGCE) sensor. MC-PNCds had a large specific surface area, which combined with the excellent electrocatalytic activity of AuNPs, synergistically improved the electrocatalytic activity. The morphology and structure of the electrode surface modifier were characterized by scanning electron microscopy, transmission electron microscopy, energy-dispersive X-ray photoelectron spectroscopy, infrared spectroscopy, X-ray diffraction, nitrogen adsorption–desorption analysis, and electrochemical characterization. Under the optimal conditions, the linear detection range of guanine (G) and adenine (A) was 0.5–160.0 μM , and the detection limits ($S/N=3$) were 72.1 and 69.6 nM, respectively. AuNPs/MC-PNCds/AGCE was successfully constructed, and was used to simultaneously detect G and A with high sensitivity and selectivity. Moreover, the sensor was successfully used to detect G and A in herring sperm DNA samples.

Keywords Metal organic frameworks · Porous nitrogen-doped carbon dodecahedron · Guanine · Adenine · Electrochemical sensor · Gold nanoparticles

Introduction

DNA, a double-helix biopolymer composed of nucleotide units, plays an important role in heart rhythm maintenance, blood flow control, neurotransmitter release inhibition, various biological metabolisms, signal transduction, and energy transduction in cells [1]. Abnormal changes in the

concentrations of the bases (e.g., guanine [G] and adenine [A], two of the four nitrogenous bases that make up DNA) in an organism may indicate immune deficiency and mutations that lead to diseases [2, 3]. In addition, the concentrations of these bases can be an important diagnostic indicator of AIDS, epilepsy, cancer, and genetic susceptibility to diseases [4, 5]. Therefore, monitoring trace levels of G and A is of great significance for studying the biological and clinical diagnosis related to genetic information and immune deficiency. Up to now, several methods have been used to determine purine base content, including high-performance liquid chromatography [6], liquid chromatography–mass spectrometry [7], gas chromatography–mass spectrometry [8], and fluorescence [9] and electrochemical analysis. Among techniques, electrochemical sensors are outstanding, with simple sample pretreatment, high detection sensitivity, and easy and simple operation [10], and thus are widely used in biomolecule analysis and detection.

For electrochemical sensors, the selection of electrocatalysts is extremely important, as it determines the sensor

✉ Yan Xu
xuyan802000@126.com

✉ Haiyun Zhai
zhaihaiyun@126.com

¹ College of Pharmacy, Guangdong Pharmaceutical University, Guangzhou 510006, China

² Key Laboratory of Digital Quality Evaluation of Chinese Materia Medica of State Administration of TCM, Guangdong Pharmaceutical University, Guangzhou 510006, China

³ Cancer Center, Integrated Hospital of Traditional Chinese Medicine, Southern Medical University, Guangzhou 510315, China

sensitivity and selectivity to a certain extent. Metal organic frameworks (MOFs) are coordination polymers that have seen rapid development in recent years, and are characterized by large pore volume, large specific surface area, open metal position, and easy functionalization [11, 12]. Moreover, MOFs can be regulated by introducing groups with different functional properties. However, the original MOFs often have defects such as low stability and weak electrocatalytic ability, which limit their practical application in electrocatalysis [13]. With further study on MOFs, derivative materials such as porous carbon, metal oxides, and metal/metal oxides have been prepared from the original MOFs as the precursor. Among these, MOF-derived carbon materials are a class of promising electrode materials with diverse morphology and structure, rich pores, high porosity, and good electrocatalytic performance. Zeolitic imidazolate frameworks (ZIFs), a new type of MOFs formed by the complexation of transition metal ions and imidazoles, have mild reaction conditions and a simple synthesis process [14]. ZIFs combine the structural advantages of natural zeolite and metal skeleton materials [15–17]. ZIFs not only can serve as a template to regulate the morphology of nanomaterial, but can also provide carbon and nitrogen sources for the construction of N-doped carbon skeleton. Zhao et al. [18] synthesized ZIF-8-derived heteroatom-doped yolk shell hierarchical porous carbon (N-CF@N) for electrochemical detection of small biomolecules. As a category of transition metal carbides, molybdenum carbide (MoC) has attracted the attention of researchers in the application of electrochemistry, owing to its good electrochemical catalytic ability and excellent conductivity [19]. For instant, Dong et al. [20] fabricated an electrochemical sensor based on Co/N-co-doped MoO₂/MoC, which was synthesized via carburizing ZIF-67-clad MoO₃ nanorods at high temperature for highly sensitive simultaneous detection of acetaminophen and 4-aminophenol, and achieved satisfactory results. Therefore, molybdate can be added to form Mo-based ZIFs (ZIF-67-MoO₄) and subsequently annealed at high temperature to obtain MoC-based porous nitrogen-doped carbon dodecahedrons (MC-PNCDs). To the best of our knowledge, there are no reports on the simultaneous detection of G and A by electrochemical sensors based on MC-PNCDs.

As one type of electrocatalyst, metal nanoparticles (NPs) such as PtNPs [21], AgNPs [22], CuNPs [23], and AuNPs [24] are widely used in electrochemical sensors. AuNPs have excellent biocompatibility, chemical stability, electrical conductivity, and catalytic performance, and are used extensively in optics, medicine, catalysis, electrochemistry, and spectroscopy. For electrochemical analysis technology, the high conductivity of NPs can be combined with many electrocatalysts to synergistically promote analytical sensitivity. For instance, the combination of NPs and porous MOFs or their derivatives can increase the load of NPs on the electrode surface, thus

synergistically increasing the electron transfer rate [25, 26]. Using the electrochemical reduction method, Ma et al. [27] prepared a ZIF-8/PtNPs/glassy carbon electrode (GCE) electrochemical sensor which was successfully applied for the sensitive detection of ascorbic acid in drugs. In this work, AuNPs with high electrocatalytic activity and stability were modified on the electrode surface by potentiostatic deposition, which further improved the electrocatalytic activity of the electrode surface. Relevant research was conducted on this basis.

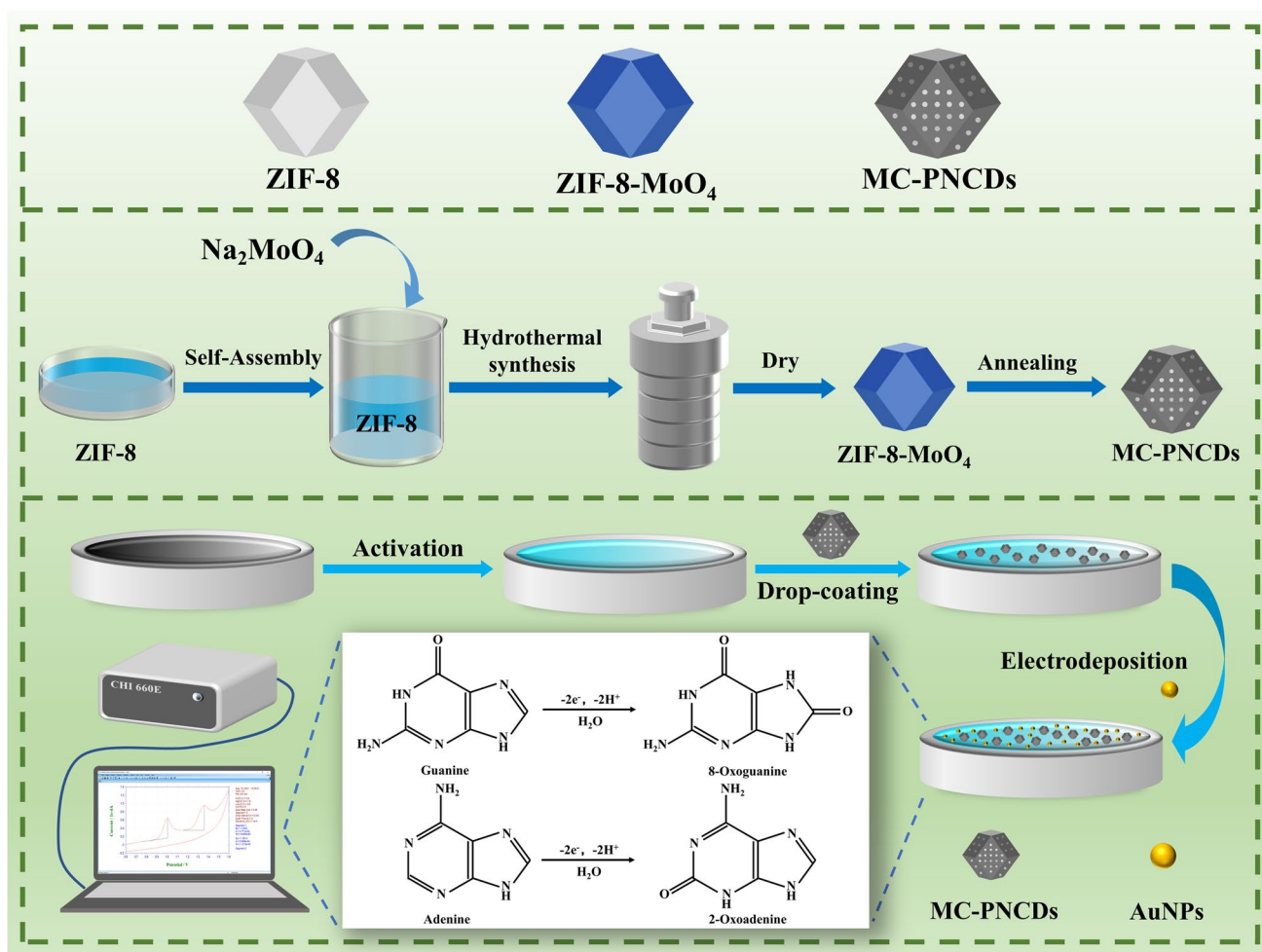
In this work, ultrafine carbide nanocrystals confined within PNCDs were synthesized by annealing ZIF-8-MoO₄. The confinement of ultrafine nanocrystals within porous nanostructures increased the contact between carbides and conductive carbon carriers, providing more stable active sites and facilitating electron transfer during oxidation reduction reactions. On this basis, we built a novel electrochemical sensor that combined AuNPs with MC-PNCDs for simultaneous detection of G and A. In addition, bare GCE can be activated for enhancing the electrochemical signal, which may be attributed to the abundant functional groups including carboxyl, carbonyl, and hydroxyl that can be induced on the surface of GCE during activation, therefore increasing the surface roughness and enhancing the electron transfer rate and electrochemical activity [28, 29]. Thus, the GCE surface was activated in phosphate buffer solution (PBS), and then the MC-PNCDs were used as the underlying support material to modify the activated GCE (AGCE). The large specific surface area and high electrical conductivity of MC-PNCDs improved the loading capacity of subsequent materials. Then, AuNPs were deposited on the surface of the MC-PNCDs/AGCE by potentiostatic deposition to form AuNPs/MC-PNCDs/AGCE (Scheme 1). The combination of MC-PNCDs and AuNPs synergistically enlarged the specific surface area, accelerated the rate of electron transfer, enhanced the conductivity, and improved the electrochemical activity of the modified electrode, which strengthened the electrochemical signal toward the targets. Morphological characterization of the electrode surface suggested that the AuNPs/MC-PNCDs/AGCE possessed large specific surface area and excellent electrocatalytic capability. The new electrochemical sensor exhibited satisfactory detection performance toward G and A, and showed high stability and selectivity. In addition, the AuNPs/MC-PNCDs/AGCE was successfully applied to detect G and A in herring sperm DNA samples.

Materials and methods

Reagents and apparatus

Chemicals and materials

Guanine, adenine, 2-methylimidazole, chloroauric acid (HAuCl₄ · 4H₂O), zinc acetate dihydrate



Scheme 1 Schematic diagram of the synthesis process of AuNPs/MC-PNCs/AGCE for electrochemical detection of G and A

$(\text{CH}_3\text{COO})_2\text{Zn}\cdot 2\text{H}_2\text{O}$), and sodium molybdate (Na_2MoO_4) were purchased from Aladdin Reagent Co., Ltd. (Shanghai, China). Disodium hydrogen phosphate (Na_2HPO_4), sodium dihydrogen phosphate (NaH_2PO_4), potassium ferricyanide ($\text{K}_3\text{Fe}(\text{CN})_6$), potassium ferrocyanide ($\text{K}_4\text{Fe}(\text{CN})_6\cdot 3\text{H}_2\text{O}$), and potassium chloride (KCl) were obtained from Sinopharm Chemical Reagent Co., Ltd. (Shanghai, China). Alumina powder was purchased from Gaoss Union, (Wuhan, China), and herring sperm was purchased from Sigma-Aldrich (St. Louis, MO, USA). All other chemicals and reagents were of analytical-grade purity unless otherwise specified, and the experimental water was deionized water.

Apparatus

Cyclic voltammetry (CV), square wave voltammetry (SWV), and chronoamperometry (i-t) were carried out on a CHI660E electrochemical workstation (Shanghai Chenhua Instrument Co., Ltd.) coupled with a conventional three-electrode system, with a GCE as working electrode, platinum electrode as counter

electrode, and saturated calomel electrode as reference electrode (Gaoss Union, Wuhan, China). Scanning electron microscopy (SEM) was used to observe the surface morphology of the modified electrode. The infrared absorption spectrum and X-ray powder diffraction (XRD) spectrum were collected using a Fourier transform infrared (FT-IR) spectrometer (Spectrum 100) (PerkinElmer, Waltham, America) and a DX-2700B diffractometer (Haoyuan, Dandong, China), respectively. All experiments were carried out at room temperature ($25^\circ\text{C} \pm 1^\circ\text{C}$).

Preparation of ZIF-8

For solution A, 2-methylimidazole (5.6 g) was dissolved in 25 mL of water and stirred at room temperature for 3 min. For solution B, zinc acetate dihydrate (1.5 g) was dissolved in 25 mL of water and stirred at room temperature for 3 min until homogenization. Then solution B was quickly added to solution A and stirred for 1 min until homogenization. The mixed solution was placed at room temperature for 48 h to form ZIF-8 dodecahedron, which

was washed three times each with dimethylformamide (DMF) and methanol. ZIF-8 was obtained after vacuum drying at 60 °C for 10 h [30].

Synthesis of MC-PNCs

MC-PNCs were prepared according to a previously reported method with minor changes [30]. First, 1.0 g of as-synthesized ZIF-8 was dispersed in 150 mL of DMF, and 1.0 g of Na₂MoO₄ was added under stirring for 10 min. The mixed solution was transferred to a 500 mL reactor for 6 h of reaction at 150 °C. The resulting white solid was centrifuged, washed three times successively with DMF and methanol, and dried at 60 °C for 12 h, forming ZIF-8-MoO₄ (white powder). The ZIF-8-MoO₄ was transferred to a tube furnace and carbonized in N₂ atmosphere. To ensure the integrity of the carbide morphology, the material was first heated from room temperature to 400 °C at a rate of 2 °C min⁻¹ for 2 h, and then heated to 800 °C at a rate of 2 °C min⁻¹ for 2 h. After cooling to room temperature, MC-PNCs were obtained (black powder).

Preparation of AuNPs/MC-PNCs/AGCE electrode

The GCE was polished on suede with alumina slurry (0.05 μm) before use, and the excess aluminum powder on the electrode surface was then washed with water. A mirror surface was formed after continuous ultrasonic treatment in ethanol and water for 2 min.

For the AGCE, the clean electrode was immersed in 0.1 M PBS (pH 7.0) and scanned by cyclic voltammetry (CV) for 10 cycles. The scanning potential was 0–1.0 V and the scanning speed was 0.10 V s⁻¹. After the electrode was removed, the excess solution on the surface was washed with water and blow-dried to form AGCE.

To prepare the MC-PNCs/AGCE, an appropriate amount of MC-PNCD powder was dispersed in water to form a 0.2 mg mL⁻¹ MC-PNCD modification solution, which was ultrasonically treated for 5 min to form an MC-PNCD suspension. Then 10 μL of the suspension was dripped onto the surface of the AGCE, which was dried at 60 °C for 15 min to form a dry film.

For the AuNPs/MC-PNCs/AGCE, the MC-PNCs/AGCE was placed in a mixed solution containing 5 mM HAuCl₄·4H₂O and 0.1 M KCl. The constant potential deposition method was applied at a potential of -0.2 V for 180 s. The deposited electrode was rinsed with water and placed at room temperature until the surface was dried to form a golden film. The AuNPs/MC-PNCs/AGCE was prepared and stored in a refrigerator at 4 °C.

Preparation of samples

For the herring sperm DNA, the DNA samples were pre-treated with 6.0 mg of DNA acidified in 2.0 mL of HCl (0.1 M) and heated in a water bath (100 °C) for 1 h. The solution was then quickly brought to room temperature in an ice bath and adjusted to the desired pH (2.0 mL, 1.0 M NaOH). Then, 0.12 mL of a denatured DNA solution was added to 10 mL of PBS, and the currents of two oxidation peaks were measured by SWV.

Results and discussion

Characterization

The surface morphology of the materials and electrodes was characterized by SEM and transmission electron microscopy (TEM). Firstly, ZIF-8 was found by SEM to be polyhedron-shaped (Fig. 1a). ZIF-8-MoO₄ prepared by anion exchange reaction had a slightly smaller size, but retained the polyhedral structure of ZIF-8 (Fig. 1b). The ZIF-8-MoO₄-derived carbide MC-PNCs maintained the polyhedron shape and further decreased in size, and the ultrafine nanocrystals were confined to the porous carbon dodecahedron (Fig. 1c and f), which was consistent with a prior report [30]. The surface of the AGCE was wrinkled and granular (Fig. 1d), and its surface microstructure changed. Figure 1e shows the SEM image of AuNPs/MC-PNCs/AGCE; by comparison, AuNPs with higher brightness and uniformly distributed on the surface of MC-PNCs/AGCE are seen, which suggested successful modification. These results confirm the successful modification of AuNPs/MC-PNCD composites on the surface of AGCE. Energy-dispersive X-ray spectroscopy (EDS) (Fig. 1g) shows that the surface of the AuNPs/MC-PNCs/AGCE was rich in carbon, nitrogen, gold, and molybdenum. Moreover, characteristic peaks of C1s, N1s, Au4d, Au4f, and Mo3d can be observed in the X-ray photoelectron spectroscopy (XPS) image (Fig. S1), indicating that AuNPs and MC-PNCs were successfully modified on the electrode surface.

The FT-IR spectrum in Fig. 1h shows the characteristic peaks of ZIF-8 at 3133 and 2927 cm⁻¹ related to the aromatic and aliphatic C–H extension of imidazole; the absorption at 1579 cm⁻¹ is due to C–N stretching; the vibrations at 1145 and 994 cm⁻¹ correspond to C–N stretching and bending, respectively. These characteristic peaks fully confirm the successful synthesis of ZIF-8 [31]. Compared with ZIF-8, ZIF-MoO₄ shows a new peak at 843.5 cm⁻¹, indicating that the MoO₄ unit successfully replaced the skeleton of ZIF-8 [30]. The main peaks in the XRD patterns of ZIF-8 correspond to the (002), (211), (220), (310), and (222) planes, and ZIF-MoO₄ showed the same results as ZIF-8 (Fig. 1i) [30, 32]. After annealing, the new peaks

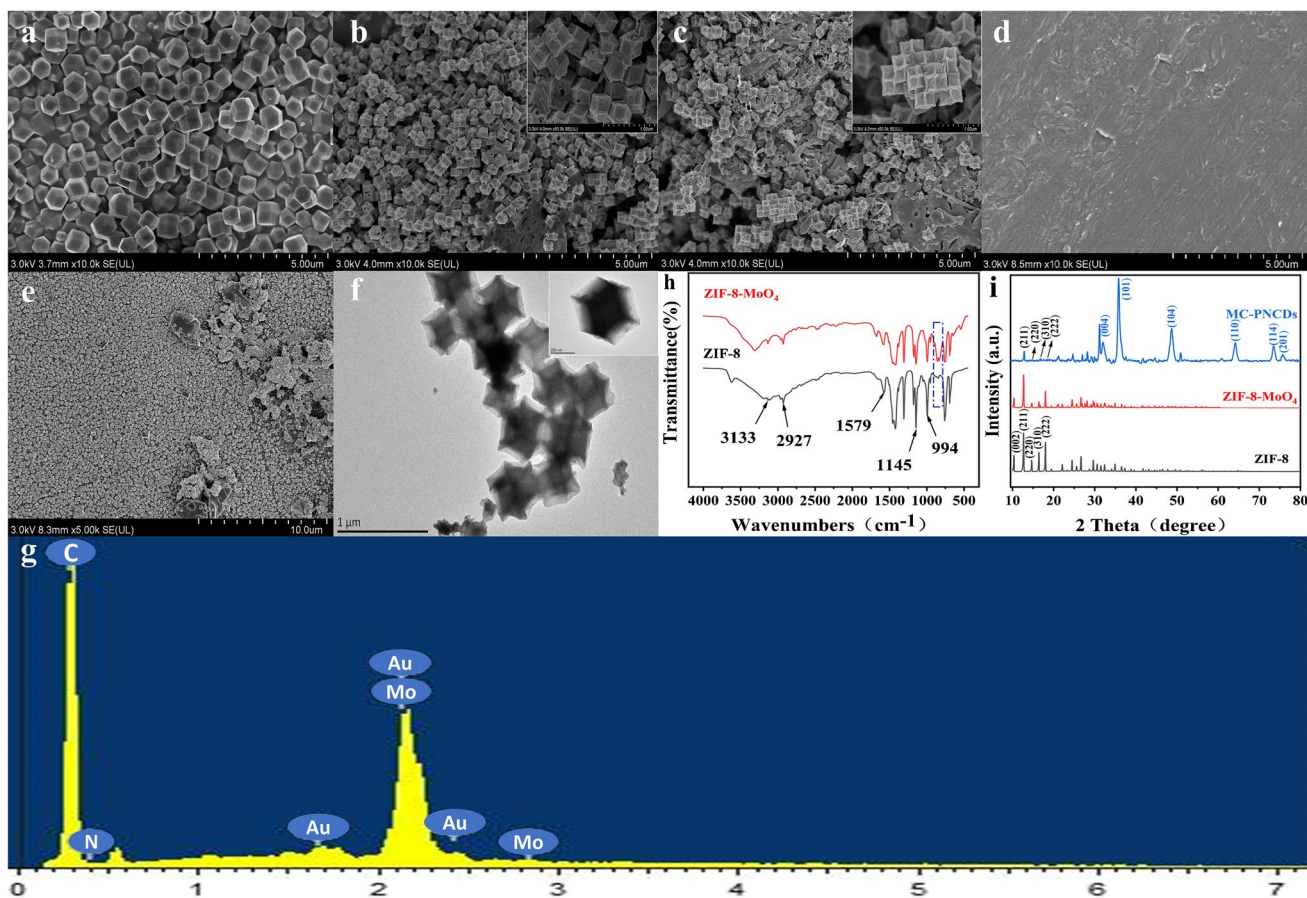


Fig. 1 SEM images of (a) ZIF-8, (b) ZIF-8-MoO₄, (c) MC-PNCs, (d) AGCE, (e) AuNPs/MC-PNCs/AGCE; (f) TEM images of MC-PNCs; (g) EDS of AuNPs/MC-PNCs/AGCE; (h) FT-IR spectrum of ZIF-8 and ZIF-8-MoO₄; (i) XRD of ZIF-8, ZIF-8-MoO₄ and MC-PNCs

of MC-PNCs corresponding to (004), (101), (104), (110), (114), and (201) were attributed to the generation of MoC, and the peaks of ZIF-8 decreased significantly, which is consistent with the results of previous reports [30, 33].

CV was used to explore the electron transfer of different modified electrodes. The GCE, AGCE, MC-PNCs/AGCE, AuNPs/AGCE, and AuNPs/MC-PNCs/AGCE electrodes were placed in a 5 mM K₃[Fe(CN)₆]/K₄[Fe(CN)₆] solution containing 0.1 M KCl to collect current curves, which were then analyzed comparatively. The black curve in Fig. 2a reveals a pair of weak reversible redox peaks on the bare electrode, corresponding to the redox reaction of ferricyanide on the electrode. The peak current of AGCE decreased significantly, indicating that activation in 0.1 M PBS solution (pH 7.0) might hinder the contact between the electrode and ferricyanide, thus weakening the current response. When MC-PNCs were modified on AGCE, the peak current increased to a certain extent. Combined with the porous structure of MC-PNCs, the modification on the electrode surface increased the effective surface area and promoted electron transfer. After electrodeposition with AuNPs on the AGCE, the peak current increased as well, owing to their

excellent conductivity, catalytic performance, and electron transfer capability. When the AuNPs were electrodeposited on the surface of the MC-PNCs/AGCE, the redox peak current increased significantly, and was larger than the other four electrodes. The results imply that AuNPs/MC-PNCs can effectively promote electron transfer on the electrode surface. Furthermore, different modified electrodes were prepared in the same solution via CV with scan rates from 10 to 250 mV s⁻¹, and their effective surface area (A_{eff}) was calculated according to the Randles–Sevcik equation [34] (Fig. S2).

$$I_p = 2.69 \times 10^5 n^{3/2} A_{eff} D^{1/2} \nu^{1/2} C$$

Herein, I_p is the corresponding peak current value, n is the number of transferred electrons during the reaction, and D presents the diffusion coefficients of 5.0 mM potassium ferricyanide solution containing 0.1 M KCl. In addition, ν and C are the scanning rate and the concentration of the electrolyte solution, respectively. It can be inferred from the formula that the A_{eff} of the AuNPs/MC-PNCs/

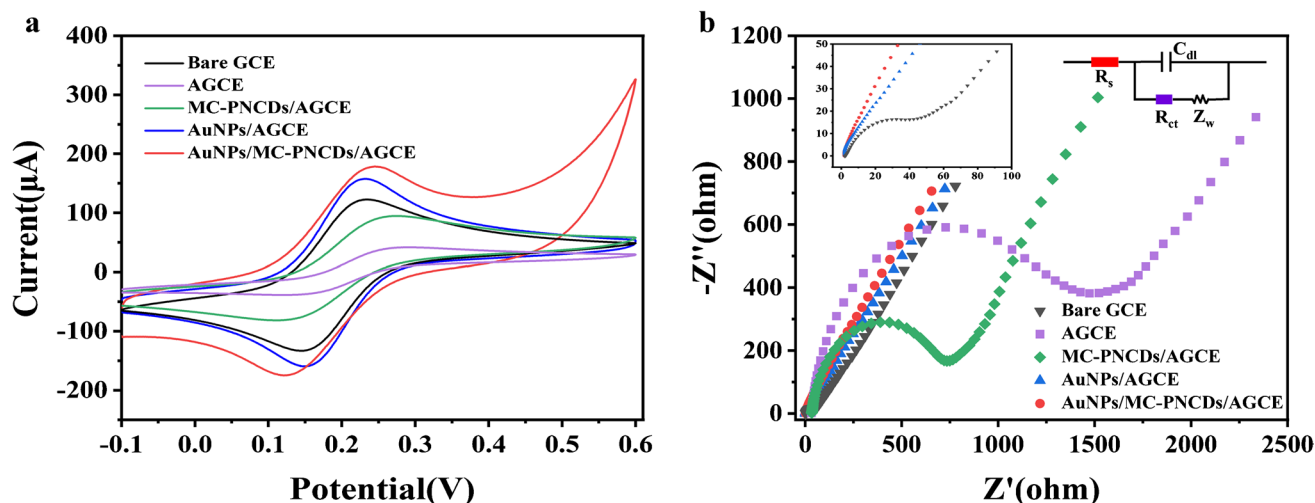


Fig. 2 CVs (a) and EIS (b) of bare GCE, AGCE, MC-PNCds/AGCE, AuNPs/AGCE, and AuNPs/MC-PNCds/AGCE in 5.0 mM $K_3[Fe(CN)_6]$ solution (containing 0.1 M KCl). Inset of Fig. 2b: the

equivalent circuit of impedance (right) and the magnified diagram of EIS curves of bare GCE, AuNPs/AGCE, and AuNPs/MC-PNCds/AGCE (left)

AGCE is 0.160 cm^2 , which is larger than that of the bare GCE (0.129 cm^2), AGCE (0.097 cm^2), MC-PNCds/AGCE (0.124 cm^2), and AuNPs/AGCE (0.143 cm^2). In addition, the Brunauer–Emmett–Teller (BET) surface area was investigated via nitrogen adsorption–desorption experiments (Fig. S3), and the BET surface area of MC-PNCds was measured as $139.3 \text{ m}^2 \text{ g}^{-1}$, suggesting the mesoporous structure of the synthesized nanocomposites. This suggests that the porosity and high surface/volume ratio of AuNPs/MC-PNCds effectively enlarged the surface area of the electrode.

Electrochemical impedance spectroscopy (EIS) was performed in 5.0 mM ferricyanide (containing 0.1 M KCl) with a potential of 0.24 V to further study the surface properties of the electrodes. As shown in Fig. 2b, the charge transfer (R_{ct}) of different modified electrodes varied significantly. Among these differences, the semicircle diameter of AGCE is much larger than that of bare GCE owing to the weakened conductivity of AGCE. When MC-PNCds or AuNPs were modified on the surface of AGCE, R_{ct} decreased, indicating that MC-PNCds increased the electron transfer rate of the electrode and promoted the excellent conductivity of the AuNPs. When AuNPs were deposited on the surface of the MC-PNCds/AGCE, the R_{ct} of the AuNPs/MC-PNCds/AGCE was further decreased, indicating that AuNPs possessed high conductivity and accelerated the electron transfer rate. The above results confirm that the AuNPs/MC-PNCds/AGCE was successfully constructed.

Electrochemical behavior of G and A at different electrodes

The CV curves of different modified electrodes at $50.0 \text{ }\mu\text{M}$ G and A (0.1 M PBS pH 2.5) were compared. G and A had

two small and wide oxidation peaks on bare GCE (Fig. 3). After activating GCE with PBS (pH 7.0) and modification with MC-PNCds or AuNPs, the peak current increased significantly, indicating that the MC-PNCds and AuNPs had a good electrochemical response to both G and A. With further electrodeposition of AuNPs on MC-PNCds, AuNPs/MC-PNCds/AGCE exhibited the largest current response among all modified electrodes, which was because the AuNPs/MC-PNCds combined the high porosity, large surface area, and good electrocatalytic performance of MC-PNCds, and the excellent conductivity and electron transfer

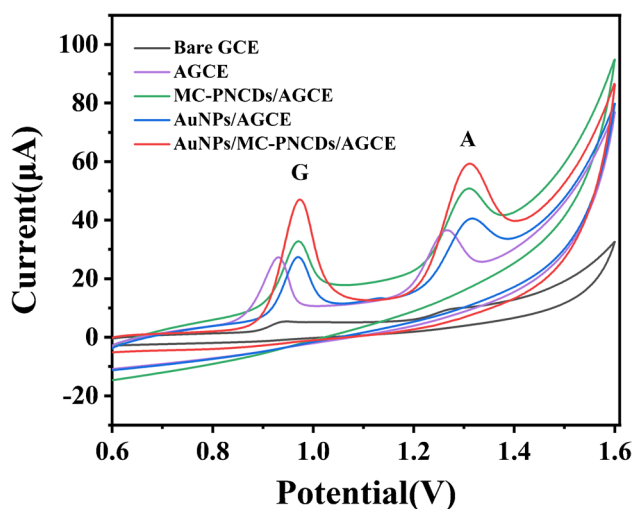


Fig. 3 CVs of bare GCE, AGCE, MC-PNCds/AGCE, AuNPs/AGCE, and AuNPs/MC-PNCds/AGCE in $50.0 \text{ }\mu\text{M}$ G and A (0.1 M PBS pH 2.5); scan rate: 0.1 V s^{-1}

capacity of AuNPs, which synergistically improved the electrochemical performance of the electrode and enhanced the electrochemical response toward the target. Therefore, the AuNPs/MC-PNCs/AGCE was used to detect G and A.

The amount of modification of the electrode surface material will affect the detection of G and A by the sensor. The modified concentration of MC-PNCs will have a moderate effect on the peak current in response to G and A. Figure S4 displays the I_p variations of 50.0 μM G and A at different modification amounts of MC-PNCs in 0.1 M PBS (pH 2.5). The oxidation peak current increased gradually with the increase in the concentration of the MC-PNCD solution. When the concentration of MC-PNCs was 2.0 mg mL^{-1} , the peak current was greatest. With a further increase in the concentration of the modification solution, the peak current decreased gradually, which might be because the excessive load of MC-PNCs led to the stacking of material, and the excessively thick modified film decreased the conductivity of the electrode, which impeded electron transfer. Therefore, the 2.0 mg mL^{-1} MC-PNCD solution was selected as the optimal modified concentration. AuNPs were deposited by potentiostatic electrodeposition on MC-PNCs/AGCE. With the variation in electrodeposition time, the amount of modified AuNPs on the electrode surface also varied, resulting in the difference in electrical signals. The detection results for 50.0 μM G and A at different deposition time (Fig. S5) showed that with the increase in electrodeposition time, the modification amount of AuNPs on the electrode surface increased. When the deposition time was 180 s, the electrical signal was highest, and the modification amount of AuNPs on the electrode surface was saturated. Therefore, 180 s was chosen as the optimal deposition time.

Influence of pH

The change in the pH of the buffer solution will change the peak current and peak potential of G and A to a certain extent, so it is necessary to optimize the pH of the buffer solution. The electrochemical behavior of 50.0 μM G and A in 0.1 M PBS (pH 1.5–4.5) was investigated by CV. The maximum peak currents of G and A were reached in the buffer at pH 2.5 (Fig. 4a and b). With a further increase in the buffer pH, the peak currents gradually decreased. Therefore, pH 2.5 was selected as the optimal pH of the buffer.

With the increase in pH, the oxidation peak potentials of G and A moved in a negative direction, indicating that protons were directly involved in this electrochemical reaction (Fig. 4c). In addition, the peak potentials (E_p) of G and A were linearly related to pH: $E_p(\text{G}) = -0.05132\text{pH} + 1.103$ ($r = 0.9991$), $E_p(\text{A}) = -0.05753\text{pH} + 1.462$ ($r = 0.9977$). The slopes of the two equations were 0.05132 and 0.05753, respectively, which were basically consistent with the standard slope value of 0.059. These results indicate that the ratio

of electron number to proton number in the electrochemical reaction of G and A on AuNPs/MC-PNCs/AGCE is about 1:1, and it is an isoprotic isoelectronic reaction.

Effect of scan rate on the electrochemical behavior of G and A

To further explore the electrochemical reaction mechanism of G and A on AuNPs/MC-PNCs/AGCE, we investigated the effect of scanning speed on the peak current and peak potential of 50.0 μM G and A through CV. As shown in Fig. 4d and e, within a scanning range of 10–250 mV s^{-1} , the oxidation peak currents of G and A gradually increased with the increase in scanning speed, and their linear relationship was as follows: $I_p(\text{A}) = 0.1566v + 6.436$ ($r = 0.9947$), $I_p(\text{G}) = 0.1147v + 2.114$ ($r = 0.9935$). The results show that the electrochemical reaction of G and A on AuNPs/MC-PNCs/AGCE is a typical adsorption control process.

At the same time, with the increase in scanning rate, the peak potentials of G and A gradually moved to the positive direction, and E_p was linearly correlated with $\ln v$ (Fig. 4f). The linear equations are as follows: $E_p(\text{A}) = 0.0280 \ln v + 1.193$ ($r = 0.9958$), $E_p(\text{G}) = 0.0220 \ln v + 0.874$ ($r = 0.9967$).

$$E_{pa} = E^\theta + \left(\frac{RT}{\alpha nF}\right) \ln \left(\frac{RTK_s}{\alpha nF}\right) + \left(\frac{RT}{\alpha nF}\right) \ln v$$

where v represents the scanning rate, α is the electron transfer coefficient, n is the number of electrons transferred, E^θ is the initial potential (V), E_{pa} is the oxidation peak potential (V), K_s is the standard rate constant (s^{-1}), R is the gas constant ($8.314 \text{ J mol}^{-1} \text{ K}^{-1}$), T represents the thermodynamic temperature (298 K), and F is the Faraday constant ($96,500 \text{ C mol}^{-1}$). For this irreversible electrochemical reaction, α can be assumed to be 0.5, from which the value of αn can be calculated, and the number of electrons transferred in the G and A electrochemical reaction can be estimated as about 2. Together with the linear relationship between E_p and pH, it can be deduced that the electrochemical reaction of G and A on AuNPs/MC-PNCs/AGCE involves two protons and two electrons. The possible reaction mechanism is shown in Fig. S6.

Determination of G and A

Under the optimal conditions, SWV was used to detect G and A at different concentrations separately and simultaneously. In a separate test, the concentration of one compound was changed and the concentration of the other remained the same. When the A concentration was fixed at 50.0 μM , with an increase in G concentration, the peak current increased as well (Fig. S7a). Within the concentration range of 0.01–150.0

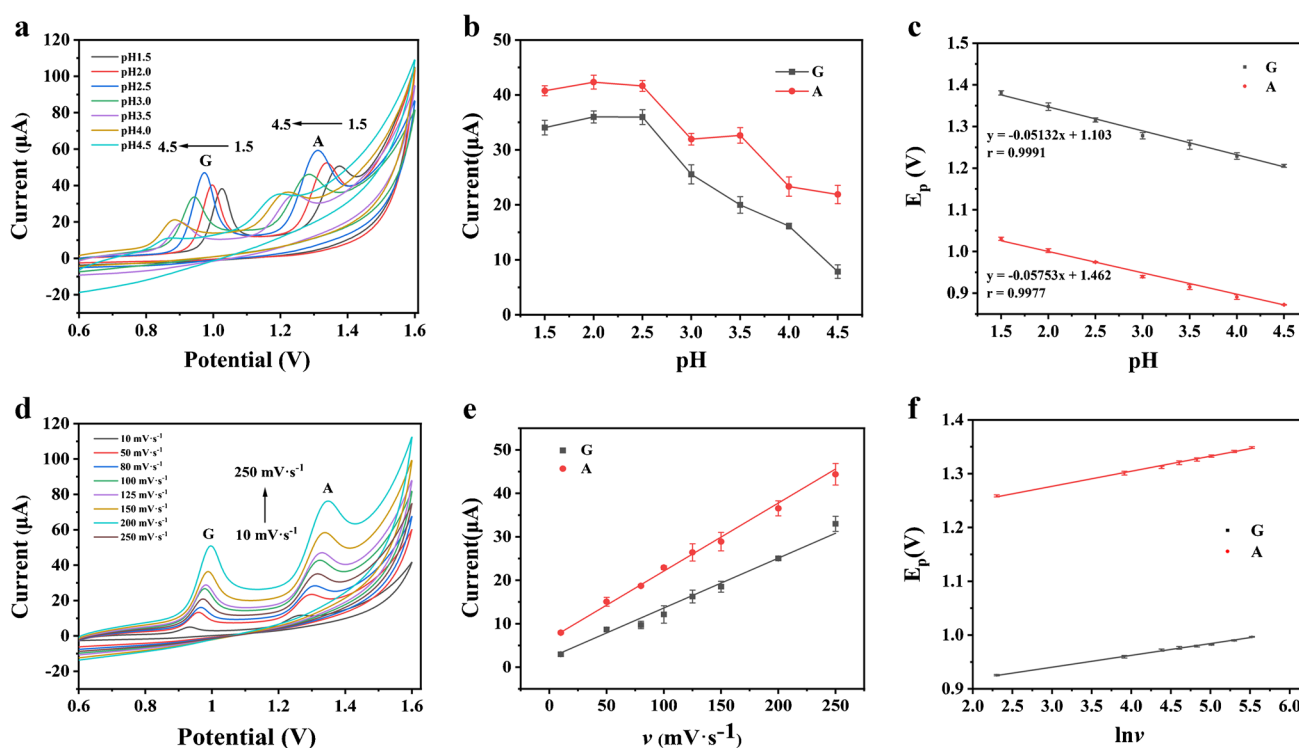


Fig. 4 (a) CVs of the AuNPs/MC-PNCDS/AGCE in the presence of 50.0 μM G and A in various pH solutions; scan rate: 0.1 V s^{-1} ; (b) the plots of pH versus peak current (I_p); (c) the plots of pH versus peak potential; (d) CVs of different scan speeds (10 mV s^{-1} to 250

mV s^{-1}) for 50.0 μM G and A in 0.1 M PBS (pH 2.5) solution; (e) the relationship between the oxidation peak current of G and A and the scanning rate ν ; (f) the linear relationship between the cathodic peak potential of 50.0 μM G and A and $\ln \nu$

μM , the linear equation of peak current and G concentration can be expressed as $I_p = 0.2665c + 0.5828$ ($R^2 = 0.9931$) (Fig. S7b). The detection limit of G ($S/N = 3$) is 69.2 nM. Similarly, when there was 50.0 μM G in the solution, the oxidation peak current increased with the increasing concentration of A and presented a good linear relationship (Fig. S7c). Within the range of 0.5–150.0 μM , the linear regression equation was $I_p = 0.2842c + 0.08419$ ($R^2 = 0.9983$) (Fig. S7d). The detection limit of A ($S/N = 3$) was 67.0 nM. The above results indicate that an increase in G or A concentration will lead to an increase in the corresponding oxidation peak current, but G and A do not interfere with each other.

To further evaluate the applicability of AuNPs/MC-PNCDS/AGCE, we detected G and A at different concentrations under the same conditions using SWV. Within the concentration range of 0.5–160.0 μM , the concentrations of G and A both showed a good linear correlation with the peak current (Fig. S7e and f). The linear regression equations are $I_p = 0.2292c + 0.2243$ ($R^2 = 0.9998$, G) and $I_p = 0.1714c + 0.0872$ ($R^2 = 0.9980$, A). The limits of detection ($S/N = 3$) for simultaneous detection of G and A were 72.1 and 69.6 nM, respectively. The above results indicate that the AuNPs/MC-PNCDS/AGCE is suitable

for detection of G and A both separately and simultaneously, and has low detection limits and wide linear ranges (Table 1).

Repeatability, reproducibility, and stability of AuNPs/MC-PNCDS/AGCE

The modified electrode was investigated by CV. The same electrode (AuNPs/MC-PNCDS/AGCE) was used to detect 50.0 μM G and A six consecutive times, and the relative standard deviations (RSDs) of the peak current were calculated as 4.5% and 4.4%, respectively. We used five electrodes (AuNPs/MC-PNCDS/AGCE) to detect 50.0 μM G and A under the same conditions, and the RSDs of the response current were 4.2% and 3.9%, respectively. The stability of the electrochemical sensor was evaluated by comparing the response of the electrode stored at 4 $^{\circ}\text{C}$ for 15 days. The peak currents of G and A were 97.4% and 96.9% of the original values, respectively (Fig. S8A). These results suggest that the electrochemical sensor has high repeatability, reproducibility, and stability.

Table 1 Comparison with other electrochemical sensors in the detection of G and A

Electrochemical sensors	Method	G		A		Reference
		Linear range (μM)	LOD (μM)	Linear range (μM)	LOD (μM)	
Cu-MOF/ERGO/GCE	DPV	0.02–10, 20–100	0.012	0.005–20, 40–200	0.002	[35]
MOF-801/MWCNT-COOH/AuNPs/GCE	DPV	0.8–60, 60–180	0.09	0.8–60, 60–180	0.08	[36]
PDA/MnO ₂ /IL-GR/GCE	DPV	10–300	0.25	10–300	0.15	[37]
COFs/NH ₂ -rG/MoS ₂ /GCE	DPV	0.5–150	0.51	1.0–280	0.44	[3]
B-CNS/GCE	SWV	0.01–0.5	0.00004	0.01–0.5	0.00002	[38]
MoxC@C/GCE	DPV	0.03–122	0.0085	0.02–122	0.008	[39]
MWCNTs-COOH/CuP-SQ COF/CoNPs/GCE	DPV	0.04–130	0.0055	0.06–130	0.0072	[5]
Cu-CeO ₂ /MWCNT/GCE	DPV	0.1–8.0	0.062	0.2–6.0	0.128	[40]
Magnetite MOF@CNT-pC/GCE	DPV	0.5–30	0.244	0.5–25	0.285	[41]
AuNPs/MC-PNCDS/AGCE	SWV	0.5–160.0	0.0721	0.5–160.0	0.0696	This work

Interference

The influence of various potentially interfering biological substances and metal ions on the anti-interference ability of the sensor in the presence of G and A was tested and the result is displayed in Fig. S8B. Within the error margin of 5%, a 50-fold increase in the concentrations of Mg²⁺, Cl⁻, K⁺, Na⁺, NO₃⁻, Zn²⁺, SO₄²⁻, sucrose, glucose, glutamic acid, ascorbic acid, uric acid, cytosine, thymine, β -cyclodextrin, and folic acid were added to 0.1 M PBS (pH 2.5) containing 50.0 μM G and A, but there was no interference (Table S1). These results confirm that the AuNPs/MC-PNCDS/AGCE has great selectivity for simultaneous determination of G and A.

Real sample analysis

To further explore the applicability of the AuNPs/MC-PNCDS/AGCE, we used the sensor to detect the content of G and A in herring sperm DNA (Fig. S9). Firstly, the herring sperm DNA was pretreated, and two oxidation peaks of G and A were clearly observed by SWV on the AuNPs/MC-PNCDS/AGCE. According to the linear regression equation, the concentrations of G and A were calculated as 28.9 and

38.1 μM , respectively. The ratio of G/A is 0.76 ($n=3$), which meets the standard of $G/A \approx 0.77$ [42]. As shown in Table 2, the recoveries of G and A were 97.7–105.0% after adding 6.0, 30.0, or 60.0 μM G and A.

Therefore, the AuNPs/MC-PNCDS/AGCE can be used to detect G and A simultaneously in herring sperm DNA.

Conclusions

In summary, a simple, sensitive electrochemical sensor based on AuNPs/MC-PNCDS/AGCE was constructed for simultaneous detection of G and A. AuNPs and MC-PNCDS synergistically enhanced the electron transfer rate and greatly improved the electrical conductivity. Modification on the surface of the AGCE further improved the electrochemical response to G and A. The sensor exhibited a wide detection range, low detection limit, and high selectivity. The sensor was successfully applied to detect purine in herring sperm DNA samples, with satisfactory results. The electrochemical sensor constructed in this experiment provides a new method for electrochemical sensor detection of G and A, and also provides a new idea for MOF-derived carbon compounds combined with NPs for electrochemical

Table 2 Determination of G and A in herring sperm DNA ($n=3$)

Sample	Analyte	Original (μM)	Added (μM)	Determined (μM)	Recovery (%)	RSD (%)
Herring sperm DNA	G	28.9	6.0	35.0	101.7	1.2
			30.0	58.2	97.7	1.9
			60.0	90.6	102.8	3.4
	A	38.1	6.0	44.4	105.0	4.4
			30.0	68.5	101.3	2.1
			60.0	98.5	100.7	1.3

sensor detection of biological small molecules. Although the fabricated electrochemical sensor obtained satisfactory results, a wider detection range and lower detection limit are further goals to pursue in our lab. At the same time, finding a higher-performance and cheaper metal to replace the noble metal (AuNPs), and therefore decreasing the detection cost and developing a more practical sensor, is an additional focus of our research.

Supplementary Information The online version contains supplementary material available at <https://doi.org/10.1007/s00216-022-04478-6>.

Acknowledgements We appreciatively acknowledge the financial support from the National Natural Science Foundation of China (NSFC, Grant No. 21005021), Natural Science Foundation of Guangdong Province (No. 2016A030313740 and No. 2021A1515011410) and Guangdong Provincial Science and Technology Project (No. 2016B030303002).

Declarations

Conflict of interest The authors declare no competing interests.

References

- Zou L, Li Y, Ye B. Voltammetric sensing of guanine and adenine using a glassy carbon electrode modified with a tetraoxocalix[2]arene[2]triazine Langmuir-Blodgett film. *Microchim Acta*. 2011;173(3-4):285–91. <https://doi.org/10.1007/s00604-011-0563-x>.
- Qin J, Gao S, Li H, Li C, Li M. Growth of monolayer and multilayer graphene on glassy carbon electrode for simultaneous determination of guanine, adenine, thymine, and cytosine. *J Electroanal Chem*. 2021;895:115403. <https://doi.org/10.1016/j.jelechem.2021.115403>.
- Zhao X, Guo H, Xue R, Wang M, Guan Q, Fan T, et al. Electrochemical sensing and simultaneous determination of guanine and adenine based on covalent organic frameworks/NH₂-rG/MoS₂ modified glassy carbon electrode. *Microchem J*. 2021;160:105759. <https://doi.org/10.1016/j.microc.2020.105759>.
- Lopes SM, Faro R, Lopes MM, Onofre I, Mendonca N, Ribeiro J, et al. Protocol for the characterization of the cytosine-adenine-guanine tract and flanking polymorphisms in Machado-Joseph disease: impact on diagnosis and development of gene-based therapies. *J Mol Diagn*. 2020;22(6):782–93. <https://doi.org/10.1016/j.jmoldx.2020.03.003>.
- Wang M, Guo H, Xue R, Guan Q, Zhang J, Zhang T, et al. A novel electrochemical sensor based on MWCNTs-COOH/metal-covalent organic frameworks (MCOFs)/Co NPs for highly sensitive determination of DNA base. *Microchem J*. 2021;167:106336. <https://doi.org/10.1016/j.microc.2021.106336>.
- Garcia del Moral P, Arin MJ, Resines JA, Diez MT. Simultaneous determination of adenine and guanine in ruminant bacterial pellets by ion-pair HPLC. *J Chromatogr B*. 2005;826(1-2):257–60. <https://doi.org/10.1016/j.jchromb.2005.07.044>.
- Cao X, Lintelmann J, Padoan S, Bauer S, Huber A, Mudan A, et al. Adenine derivatization for LC-MS/MS epigenetic DNA modifications studies on monocytic THP-1 cells exposed to reference particulate matter. *Anal Biochem*. 2021;618:114127. <https://doi.org/10.1016/j.ab.2021.114127>.
- Glavin DP, Cleaves HJ, Buch A, Schubert M, Aubrey A, Bada JL, et al. Sublimation extraction coupled with gas chromatography-mass spectrometry: A new technique for future in situ analyses of purines and pyrimidines on Mars. *Planet Space Sci*. 2006;54(15):1584–91. <https://doi.org/10.1016/j.pss.2005.12.023>.
- Cywinski PJ, Moro AJ, Ritschel T, Hildebrandt N, Lohmannsroben HG. Sensitive and selective fluorescence detection of guanine nucleotides by nanoparticles conjugated with a naphthyridine receptor. *Anal Bioanal Chem*. 2011;399(3):1215–22. <https://doi.org/10.1007/s00216-010-4420-2>.
- Zhu W, Zhou Y, Tao M, Yan X, Liu Y, Zhou X. An electrochemical and fluorescence dual-signal assay based on Fe₃O₄@MnO₂ and N-doped carbon dots for determination of hydrogen peroxide. *Microchim Acta*. 2020;187(3):187. <https://doi.org/10.1007/s00604-020-4163-5>.
- Gao F, Tu X, Ma X, Xie Y, Zou J, Huang X, et al. NiO@Ni-MOF nanoarrays modified Ti mesh as ultrasensitive electrochemical sensing platform for luteolin detection. *Talanta*. 2020;215:120891. <https://doi.org/10.1016/j.talanta.2020.120891>.
- Lu Z, Zhong J, Zhang Y, Sun M, Zou P, Du H, et al. MOF-derived Co₃O₄/FeCo₂O₄ incorporated porous biomass carbon: Simultaneous electrochemical determination of dopamine, acetaminophen and xanthine. *J Alloys Compd*. 2021;858:157701. <https://doi.org/10.1016/j.jallcom.2020.157701>.
- Khaletskaya K, Pougin A, Medishetty R, Rösler C, Wiktor C, Strunk J, et al. Fabrication of gold/titania photocatalyst for CO₂ reduction based on pyrolytic conversion of the metal-organic framework NH₂-MIL-125(Ti) loaded with gold nanoparticles. *Chem Mater*. 2015;27(21):7248–57. <https://doi.org/10.1021/acs.chemmater.5b03017>.
- Lgaz H, Lee H-s. Computational investigation on interaction mechanism of sulfur mustard adsorption by zeolitic imidazolate frameworks ZIF-8 and ZIF-67: Insights from periodic and cluster DFT calculations. *J Mol Liq*. 2021;344:117705. <https://doi.org/10.1016/j.molliq.2021.117705>.
- Chen X, Zhao J-X, Wang J-W, Liu Y, Wang L-C, Weerasooriya R, et al. Doping ZIF-67 with transition metals results in bimetallic centers for electrochemical detection of Hg(II). *Electrochim Acta*. 2021;387:138539. <https://doi.org/10.1016/j.electacta.2021.138539>.
- Ma F, Jin S, Li Y, Feng Y, Tong Y, Ye B-C. Pyrolysis-derived materials of Mn-doped ZIF-67 for the electrochemical detection of o-nitrophenol. *J Electroanal Chem*. 2022;904:115932. <https://doi.org/10.1016/j.jelechem.2021.115932>.
- Mo G, Zheng X, Ye N, Ruan Z. Nitrogen-doped carbon dodecahedron embedded with cobalt nanoparticles for the direct electro-oxidation of glucose and efficient nonenzymatic glucose sensing. *Talanta*. 2021;225:121954. <https://doi.org/10.1016/j.talanta.2020.121954>.
- Zhao G, Wang T, Li L, Tang Y, Qin Q, Wu C. Heteroatoms doped yolk-shell hierarchically porous carbon derived from ZIF-8 for electrochemical sensing. *Carbon*. 2021;183:291–300. <https://doi.org/10.1016/j.carbon.2021.07.017>.
- Keerthika Devi R, Ganesan M, Chen TW, Chen SM, Lin KY, Akilarasan M, et al. Tailored architecture of molybdenum carbide/iron oxide micro flowers with graphitic carbon nitride: An electrochemical platform for nano-level detection of organophosphate pesticide in food samples. *Food Chem*. 2022;397:133791. <https://doi.org/10.1016/j.foodchem.2022.133791>.
- Dong Y, Zhou M, Zhang L. 3D multiporous Co,N co-doped MoO₂/MoC nanorods hybrids as improved electrode materials for highly sensitive simultaneous determination of acetaminophen and 4-aminophenol. *Electrochim Acta*. 2019;302:56–64. <https://doi.org/10.1016/j.electacta.2019.02.006>.
- Yuan MM, Zou J, Huang ZN, Peng DM, Yu JG. PtNPs-GNPs-MWCNTs-beta-CD nanocomposite modified glassy carbon electrode for sensitive electrochemical detection of folic acid. *Anal Bioanal Chem*. 2020;412(11):2551–64. <https://doi.org/10.1007/s00216-020-02488-w>.

22. Achraf Ben Njima M, Legrand L. Ag nanoparticles-oxidized green rust nanohybrids for novel and efficient non-enzymatic H₂O₂ electrochemical sensor. *J Electroanal Chem.* 2022;906:116015. <https://doi.org/10.1016/j.jelechem.2022.116015>.
23. Zhou ZF, Feng XZ, Zhan T, Han GC, Chen Z, Kraatz HB. Facile bimetallic co-amplified electrochemical sensor for folic acid sensing based on CoNPs and CuNPs. *Anal Bioanal Chem.* 2022;414(23):6791–800. <https://doi.org/10.1007/s00216-022-04242-w>.
24. Jiang Y, Zhao H, Zhu N, Lin Y, Yu P, Mao L. A simple assay for direct colorimetric visualization of trinitrotoluene at picomolar levels using gold nanoparticles. *Angew Chem Int Edit.* 2008;47(45):8601–4. <https://doi.org/10.1002/anie.200804066>.
25. Dong H, Liu S, Liu Q, Li Y, Li Y, Zhao Z. A dual-signal output electrochemical immunosensor based on Au-MoS₂/MOF catalytic cycle amplification strategy for neuron-specific enolase ultrasensitive detection. *Biosens Bioelectron.* 2022;195:113648. <https://doi.org/10.1016/j.bios.2021.113648>.
26. Wu J, Wu Y, Lu L, Zhang D, Wang X. Single-atom Au catalyst loaded on CeO₂: A novel single-atom nanozyme electrochemical H₂O₂ sensor. *Talanta Open.* 2021;4:100075. <https://doi.org/10.1016/j.talo.2021.100075>.
27. Ma Y, Zhang Y, Wang L. An electrochemical sensor based on the modification of platinum nanoparticles and ZIF-8 membrane for the detection of ascorbic acid. *Talanta.* 2021;226:122105. <https://doi.org/10.1016/j.talanta.2021.122105>.
28. Rahman MM, Ahmed A, Lee J-J. A conducting poly(N-(1-naphthyl)ethylenediamine dihydrochloride) nanofibers for the sensitive and interference-free detection of dopamine. *J Electrochem Soc.* 2018;165(3):B89–95. <https://doi.org/10.1149/2.0421803jes>.
29. Lu Y, Bao C, Zou J, Xiao J, Zhong W, Gao Y. Highly sensitive electrochemical sensor for sunset yellow based on electrochemically activated glassy carbon electrode. *Molecules.* 2022;27(16):5221. <https://doi.org/10.3390/molecules27165221>.
30. Lu XF, Yu L, Zhang J, Lou XWD. Ultrafine dual-phased carbide nanocrystals confined in porous nitrogen-doped carbon dodecahedrons for efficient hydrogen evolution reaction. *Adv Mater.* 2019;31(30):1900699. <https://doi.org/10.1002/adma.201900699>.
31. Ge Y, Wang K, Liu J, Tian Y, Li H, Wang H, et al. A ZIF-8-based multifunctional intelligent drug release system for chronic osteomyelitis. *Colloid Surface B.* 2022;212:112354. <https://doi.org/10.1016/j.colsurfb.2022.112354>.
32. Gao F, Yang J, Tu X, Yu Y, Liu S, Li M, et al. Facile synthesis of ZIF-8@poly(3,4-ethylenedioxythiophene):poly(4-styrenesulfonate) and its application as efficient electrochemical sensor for the determination dichlorophenol. *Synth Met.* 2021;277:116769. <https://doi.org/10.1016/j.synthmet.2021.116769>.
33. Lin Q, Shang C, Chen Z, Wang X, Zhou G. Boron-doped molybdenum carbide as a pH-independent electrocatalyst for the hydrogen evolution reaction. *Int J Hydrogen Energ.* 2020;45(55):30659–65. <https://doi.org/10.1016/j.ijhydene.2020.08.033>.
34. He B, Yan X. An amperometric zearalenone aptasensor based on signal amplification by using a composite prepared from porous platinum nanotubes, gold nanoparticles and thionine-labelled graphene oxide. *Microchim Acta.* 2019;186(6):383. <https://doi.org/10.1007/s00604-019-3500-z>.
35. Wang X, Zhang J, Wei Y, Xing T, Cao T, Wu S, et al. A copper-based metal-organic framework/graphene nanocomposite for the sensitive and stable electrochemical detection of DNA bases. *Analyst.* 2020;145(5):1933–42. <https://doi.org/10.1039/c9an02398d>.
36. Guo H, Zhang T, Wang M, Sun L, Zhang J, Yang M, et al. Electrochemical behavior of MOF-801/MWCNT-COOH/AuNPs: A highly selective electrochemical sensor for determination of guanine and adenine. *Colloid Surface A.* 2021;627:127195. <https://doi.org/10.1016/j.colsurfa.2021.127195>.
37. Zhang S, Zhuang X, Chen D, Luan F, He T, Tian C, et al. Simultaneous voltammetric determination of guanine and adenine using MnO₂ nanosheets and ionic liquid-functionalized graphene combined with a permeation-selective polydopamine membrane. *Microchim Acta.* 2019;186(7):450. <https://doi.org/10.1007/s00604-019-3577-4>.
38. Emran MY, El-Safty SA, Selim MM, Shenashen MA. Selective monitoring of ultra-trace guanine and adenine from hydrolyzed DNA using boron-doped carbon electrode surfaces. *Sensor Actuat B-Chem.* 2021;329:129192. <https://doi.org/10.1016/j.snb.2020.129192>.
39. Zhang L, Zhang J. Multiporous molybdenum carbide nanosphere as a new charming electrode material for highly sensitive simultaneous detection of guanine and adenine. *Biosens Bioelectron.* 2018;110:218–24. <https://doi.org/10.1016/j.bios.2018.03.064>.
40. Aktürk M, Karabiberoglu ŞU, Dursun Z. Fabrication of Cu–CeO₂ coated multiwall carbon nanotube composite electrode for simultaneous determination of guanine and adenine. *Electroanal.* 2018;30(2):238–49. <https://doi.org/10.1002/elan.20170590>.
41. Şenocak A, Tümay SO, Ömeroğlu İ, Şanko V. Crosslinker polycarbazole supported magnetite MOF@CNT hybrid material for synergetic and selective voltammetric determination of adenine and guanine. *J Electroanal Chem.* 2022;905. <https://doi.org/10.1016/j.jelechem.2021.115963>.
42. Ng KL, Khor SM. Graphite-based nanocomposite electrochemical sensor for multiplex detection of adenine, guanine, thymine, and cytosine: a biomedical prospect for studying DNA damage. *Anal Chem.* 2017;89(18):10004–12. <https://doi.org/10.1021/acs.analchem.7b02432>.

Publisher's note Springer Nature remains neutral with regard to jurisdictional claims in published maps and institutional affiliations.

Springer Nature or its licensor (e.g. a society or other partner) holds exclusive rights to this article under a publishing agreement with the author(s) or other rightsholder(s); author self-archiving of the accepted manuscript version of this article is solely governed by the terms of such publishing agreement and applicable law.